

NON-GAUSSIAN SCATTER IN CLUSTER SCALING RELATIONS

LAURIE D. SHAW, GILBERT P. HOLDER AND JONATHAN DUDLEY

Department of Physics, McGill University, Montreal QC H3A 2T8

Draft version October 22, 2018

ABSTRACT

We investigate the impact of non-Gaussian scatter in the cluster mass-observable scaling relation on the mass and redshift distribution of clusters detected by wide area surveys. We parameterize non-Gaussian scatter by incorporating the third and fourth moments (skewness and kurtosis) into the distribution $P(M_{\text{obs}}|M)$. We demonstrate that for low scatter mass proxies the higher order moments do not significantly affect the observed cluster mass and redshift distributions. However, for high scatter mass indicators it is necessary for the survey limiting mass threshold to be less than $10^{14}h^{-1}M_{\odot}$ to prevent the skewness from having a significant impact on the observed number counts, particularly at high redshift. We also show that an unknown level of non-Gaussianity in the scatter is equivalent to an additional uncertainty on the variance in $P(M_{\text{obs}}|M)$ and thus may limit the constraints that can be placed on the dark energy equation of state parameter w . Furthermore, positive skewness flattens the mass function at the high mass end, and so one must also account for skewness in $P(M_{\text{obs}}|M)$ when using the shape of the mass function to constrain cluster scaling-relations.

Subject headings: cosmology: dark matter — galaxies: clusters: general — intergalactic medium

1. INTRODUCTION

The evolution of the number density of galaxy clusters is a sensitive cosmological probe (Bahcall & Fan 1998; Eke et al. 1998). As an indicator of the expansion rate as a function of time, the galaxy cluster number density is sensitive to the dark energy equation of state (Haiman et al. 2001; Weller et al. 2001). This provides a growth-based dark energy test, an important complement to the distance-based tests that have provided the most compelling evidence for dark energy to this point (Perlmutter et al. 1999; Schmidt et al. 1998).

Galaxy clusters can be selected by many diverse methods, including (but not limited to) optical richness, X-ray thermal bremsstrahlung flux, weak lensing shear and the Sunyaev-Zel'dovich (SZ) effect. The key challenge for using galaxy clusters as precise cosmological probes is in understanding how to relate observables to a quantity that can be well predicted by theory, for example, mass. The ultimate goal is to produce theoretical predictions of the distributions of observables as a function of redshift and cosmological parameters. Short of this, one approach is to theoretically model the evolution of number density as a function of mass, and then estimate the mapping between observables and mass in order to predict the observed evolution. This mapping can either be estimated from theoretical considerations or be determined directly from the data, assuming some regularity in the mapping (Majumdar & Mohr 2003; Hu 2003; Lima & Hu 2004, 2005).

It is important to understand the statistics of the relevant mass-observable scaling relation. Although clusters may follow a mean relation, individual clusters will deviate from it. If the level of scatter around the mean relation is not small, the shape and amplitude of the observed mass function can change significantly. At cluster scales the mass-function is a steeply declining function of

mass. Therefore a larger number of low mass clusters will scatter over the detection threshold of the survey than those higher mass clusters that scatter below it. The net increase in the total number of clusters in the sample is thus dependent on the slope of the mass function at the threshold mass, and the magnitude of the scatter around the mass-observable scaling relation. If the latter is well constrained then the measurement of the cluster mass-function is actually improved statistically due to the reduction in shot noise. However, in practice it is difficult to precisely measure the scatter and theoretical estimates can vary substantially. Furthermore, as we shall demonstrate, for large intrinsic scatter, the magnitude of the higher order moments (skewness and kurtosis) can become significant.

Previous work forecasting the constraints on cosmological parameters that can be achieved by cluster surveys have assumed the scatter in scaling relations to be log-normally distributed around the mean relation (that is, normally distributed in the logarithm of the mass). However, cosmological simulations and observations of large samples of clusters have demonstrated deviations from lognormal behaviour. In general, the cause of these deviations can be separated into two categories; dynamical state and projection effects.

The former refers to the impact of a sub-population of clusters that are systematically offset from the mean scaling relation due to their dynamical state. Shaw et al. (2006) and Evrard et al. (2008) demonstrated using N-body simulations that dark matter halos undergoing a major merger have a systematically higher dark matter velocity dispersion (σ_{DM}) than their more relaxed counterparts (of the same mass). Evrard et al. (2008) showed that the small fraction of interacting halos cause positive skewness in the distribution of the residuals around the *mass* – σ_{DM} relation. Stanek et al. (2009) analyse the covariance of bulk cluster properties using a large sample of halos extracted from hydrodynamical simula-

tions. They find small deviations from Gaussian scatter for some properties, most notably in the mass-weighted temperature – mass relation. Pratt et al. (2009) analysed X-ray luminosity scaling relations using a sample of 31 nearby clusters observed by the XMM-Newton X-ray observatory. They find that the scatter in the $L_x - Y_X$ relation (where Y_X was assumed to be a robust, low scatter proxy for cluster mass) was significantly non-Gaussian due to the systematically above-average luminosity of cooling core clusters in their sample. They also note that the scatter becomes more Gaussian when the central regions of the clusters are excluded in the luminosity measurements.

The second cause of non-Gaussianity in observed scaling relations is confusion in cluster selection due to projection effects. Several studies have demonstrated that lower mass, unresolved clusters, as well as gas outwith cluster regions can contribute significantly to the measured integrated SZ flux (Y), causing additional scatter in the $Y - M$ relation and introducing a tail towards high flux in the distribution of Y at constant mass (White et al. 2002; Holder et al. 2007; Hallman et al. 2007). A similar effect is found for optically-selected clusters. Cohn et al. (2007) demonstrated using mock galaxy catalogues that a non-negligible fraction of clusters (10% at $z = 0.4$ to 22% at $z = 1$) identified using the red-sequence are ‘blends’ – cluster candidates in which a large number of different halos have contributed galaxies. Blends thus cause a tail towards high richness in the distribution of optical richness at fixed mass.

In this work, we relax the assumption of lognormal scatter and investigate the effect of non-Gaussian scatter around the mean mass-observable scaling relation on the observed mass and redshift distribution of clusters. Specifically, we quantify the impact of non-zero skewness and kurtosis – the third and fourth standardized moments of a generalized probability distribution – as perturbations to the purely Gaussian case.

Throughout this paper we make a distinction between *true* mass M and *observed* mass M_{obs} . The former is the actual cluster mass, as defined by a spherical overdensity, Δ , and measured in cosmological simulations of structure formation (Jenkins et al. 2001; Warren et al. 2006; Tinker et al. 2008). M_{obs} is the cluster mass that would be inferred from observations through application of a scaling relation (e.g. $Y - M$, $L_x - M$, etc), or via self-calibration of the mass function (Lima & Hu 2005; Cunha 2009).

2. SCATTER IN THE MASS-OBSERVABLE SCALING RELATION

The predicted redshift distribution of clusters observed by a given survey is given by

$$\frac{dN}{dz} = \Delta\Omega \frac{dV}{dzd\Omega}(z) \int_0^\infty \frac{dM}{M} \frac{d\bar{n}}{d\ln(M)} f(M, z), \quad (1)$$

where M is cluster mass and $d\bar{n}/d\ln M$ is the mean comoving number density of clusters (the mass function). The function $f(M_{\text{lim}}, z)$ represents the survey selection function which accounts for the limiting mass of the survey, M_{lim} defined by some threshold in the mass observable (e.g. optical richness, X-ray luminosity, integrated SZ flux), and the statistics of the mapping between M_{obs} and M . In the limit of perfect (zero scatter)

mass measurements, this is simply a step function at the limiting mass of the survey.

If one assumes lognormal scatter around the mean scaling relation (Gaussian scatter in $\ln M$) then the probability $P(M_{\text{obs}}|M)$ of observing the mass M_{obs} given the “true” underlying mass M , is

$$P(M_{\text{obs}}|M) = \frac{1}{\sqrt{2\pi\sigma_{\ln M}^2}} \exp[-x^2(M_{\text{obs}})], \quad (2)$$

with

$$x(M_{\text{obs}}) \equiv \frac{\ln M_{\text{obs}} - \ln M - \ln M_{\text{bias}}}{\sqrt{2\sigma_{\ln M}^2}}. \quad (3)$$

This parameterization allows for redshift dependent scatter $\sigma_{\ln M}$ and bias M_{bias} in the mass-observable scaling relation (Lima & Hu 2005; Cunha 2009). For simplicity, we henceforth ignore the bias term and concentrate on the impact of scatter alone. The distribution of observed cluster masses is just a convolution of the true mass function with $P(M_{\text{obs}}|M)$,

$$\frac{d\bar{n}}{d\ln M_{\text{obs}}} = \int_0^\infty \frac{d\bar{n}}{d\ln M} P(M_{\text{obs}}|M) d\ln M. \quad (4)$$

Plugging in Eqn. 2 and assuming an intrinsic power law distribution in mass, $d\bar{n}/d\ln(M) \propto M^{-\alpha}$, it is straightforward to show that the observed mass distribution is

$$\frac{d\bar{n}}{d\ln M_{\text{obs}}} = \left(\frac{d\bar{n}}{d\ln M} \right)_\circ e^{(\alpha^2\sigma_{\ln M}^2/2)}, \quad (5)$$

where \circ denotes the true mass distribution evaluated at M_{obs} by applying the mean $M - M_{\text{obs}}$ scaling relation.

The extent of the deviation of the observed mass function from the true mass function is clearly controlled by $\alpha\sigma_{\ln M}$, the product of the standard deviation of the distribution $P(M_{\text{obs}}|M)$ with the slope of the mass function, α . Evidently, a constant $\alpha\sigma_{\ln M}$ results in an observed mass function that has a constant and positive vertical offset from the true mass function. For more realistic mass functions (Jenkins et al. 2001; Tinker et al. 2008) the slope α is approximately 1 at the group mass scale and increases with increasing mass and redshift, exponentially so at very high mass and redshift. The impact of scatter on the observed mass function is thus significantly greater at high masses/redshifts (see Section 3).

Above a limiting threshold in M_{obs} , scatter in a cluster scaling relation causes a net increase in the number of detected clusters. An unknown amount of scatter in the scaling relation thus degrades the cosmological constraints that can be obtained from cluster number counts as one must also marginalise over $\sigma_{\ln M}$. Lima & Hu (2005) demonstrated that for a survey with a fixed limiting mass of $10^{14.2}h^{-1}M_\odot$ and $\sigma_{\ln M}^2 = 0.25^2$, a 1σ uncertainty of 0.25^2 on $\sigma_{\ln M}^2$ would produce a 10% uncertainty in the number counts at $z = 0.5$, a 20% uncertainty at $z = 1$, and a 50% uncertainty at $z = 2$.

2.1. Non-Gaussian Scatter

We now determine the impact on the observed mass function of non-Gaussian scatter in the mass-observable relation. We proceed by using the Edgeworth series to approximate a non-Gaussian $P(M_{\text{obs}}|M)$

(e.g. Bernardeau & Kofman 1995; Blinnikov & Moessner 1998), thus taking it to be a perturbation to the Gaussian case. It is parameterised by the third and fourth moments, the skewness (γ) and kurtosis (κ), of the probability distribution $P(M_{\text{obs}}|M)$. The Edgeworth expansion is particularly useful for convolutions when expressed as a series of derivatives of Gaussians,

$$P(M_{\text{obs}}|M) \approx G(x) - \frac{\gamma}{6} \frac{d^3 G}{dx^3} + \frac{\kappa}{24} \frac{d^4 G}{dx^4} + \frac{\gamma^2}{72} \frac{d^6 G}{dx^6} \quad (6)$$

where the skewness, γ is defined as

$$\gamma = \frac{\langle (M_{\text{obs}} - M)^3 \rangle}{\sigma^3} \quad (7)$$

and the kurtosis, κ as

$$\kappa = \frac{\langle (M_{\text{obs}} - M)^4 \rangle}{\sigma^4} - 3, \quad (8)$$

and $G(x)$ is a Gaussian distribution in x (equal to $P(M_{\text{obs}}|M)$ in Eq. 2).

By plugging Equation 6 into Equation 4 and doing some integration by parts, the observed mass function can be calculated for any true mass function,

$$\begin{aligned} \frac{d\bar{n}}{d \ln M_{\text{obs}}} &= \int \frac{d\bar{n}}{dx} G(x) dx - \frac{\gamma}{6} \int \frac{d^3}{dx^3} \left(\frac{d\bar{n}}{dx} \right) G(x) dx \\ &+ \frac{\kappa}{24} \int \frac{d^4}{dx^4} \left(\frac{d\bar{n}}{dx} \right) G(x) dx \\ &+ \frac{\gamma^2}{72} \int \frac{d^6}{dx^6} \left(\frac{d\bar{n}}{dx} \right) G(x) dx + \dots \quad (9) \end{aligned}$$

Assuming again an intrinsic power-law distribution of mass with slope α , $d\bar{n}/d \ln M_{\text{true}} = M^{-\alpha}$, it is straightforward to show that the observed mass distribution is now

$$\begin{aligned} \frac{d\bar{n}}{d \ln M_{\text{obs}}} &= \left(\frac{d\bar{n}}{d \ln M} \right)_{\circ} e^{\alpha^2 \sigma^2 / 2} \times \\ &\left[1 + \frac{\alpha^3 \sigma^3}{6} \gamma + \frac{\alpha^4 \sigma^4}{24} \kappa + \frac{\alpha^6 \sigma^6}{72} \gamma^2 \right], \quad (10) \end{aligned}$$

where \circ denotes the true mass distribution evaluated at M_{obs} .

The relevant parameter here is again clearly $\alpha \sigma_{\ln M}$. If this parameter is large, there are two important effects: the number of objects at any given mass scale is increased substantially (as for the Gaussian case), and the higher order moments of the distribution, γ and κ , become important. The transition at which the latter occurs is clearly when $\alpha \sigma_{\ln M}$ becomes greater than unity. For example, if $\alpha \sigma_{\ln M} = 1$, then $\gamma = 1$ produces an 17% increase on the number counts compared to the purely Gaussian case at any given mass scale. Assuming $\kappa = 1$ provides an additional 4% correction. Note that Equation 10 demonstrates that both (positive) γ and κ cause an up-scattering of clusters. For skewness this is due to the tail towards large mass that increases the probability of a cluster of having $M_{\text{obs}} \gg M$. For kurtosis, the up-scattering is due to the wider wings of the distribution.

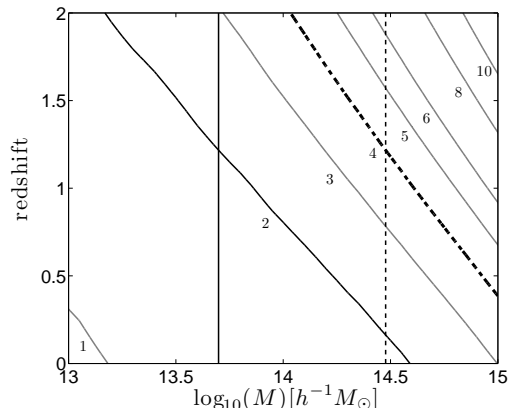


FIG. 1.— Contours of constant slope, α of the halo mass function, where $d\bar{n}/d \ln(M) \propto M^{-\alpha}$, as a function of mass and redshift for our fiducial cosmology. The solid black contour emphasizes the critical curve $M_c(z)$ (see text) for a DES-like optical survey ($\sigma_{\ln M} = 0.5$), the black dashed contour shows $M_c(z)$ for an SPT-like SZ survey ($\sigma_{\ln M} = 0.25$). The black solid and dashed vertical lines show the assumed limiting masses for the DES and SPT surveys, respectively.

3. IMPLICATIONS OF NON-GAUSSIAN SCATTER FOR SZ AND OPTICAL CLUSTER SURVEYS

We now evaluate the impact of non-Gaussian scatter in the mass-observable scaling relation on the predicted mass and redshift distribution of clusters observed by a South Pole Telescope-like SZ survey and a Dark Energy Survey-like optical survey. For the SZ survey we assume that the scatter in the mass-SZ flux relation is $\sigma_{\text{SZ}} = 0.25$ (Shaw et al. 2008) and the limiting mass is $3 \times 10^{14} h^{-1} M_{\odot}$. For the optical survey we assume the scatter in the optical richness - mass relation is $\sigma_{\text{opt}} = 0.5$, in keeping with the results of Rykoff et al. (2008a,b); Becker et al. (2007); Rozo et al. (2009, 2008), and a constant limiting mass of $5 \times 10^{13} h^{-1} M_{\odot}$. Note that Becker et al. (2007) found that the scatter in the richness-mass relation is 0.5-0.75, and we have taken the value at the lower end of this range.

We have demonstrated that the impact of the higher order moments γ and κ become significant when $\sigma_{\ln M} \alpha$, the product of the slope of the mass function and the standard deviation of $P(M_{\text{obs}}|M)$, becomes greater than unity. Under the simplifying assumption that $\sigma_{\ln M}$ is independent of mass and redshift for a given observable, the higher order moments thus become relevant when the effective slope of the mass function exceeds the threshold value, $\alpha_c > 1/\sigma_{\ln M}$. This critical slope is reached above a redshift (and cosmology) dependent mass threshold $M_c(z)$. For SPT, $\alpha_{c,\text{SZ}} = 1/0.25 = 4$, for DES $\alpha_{c,\text{opt}} = 2$.

In Figure 1 we plot the slope of the mass function as a function of mass and redshift. For this, we adopt the mass function of Tinker et al. (2008), and assuming $d\bar{n}/d \ln(M) \propto M^{-\alpha}$ at any given mass and redshift, calculate α over a wide range of mass and redshift. The mass function is defined in terms of M_{200} , where the subscript denotes the mass enclosed in the region of spherical overdensity of 200 times the *mean* density of the Universe (at the relevant redshift). For our fiducial cosmology we assume parameters consistent with the WMAP 5-year results ($\Omega_M = 0.27$, $\sigma_8 = 0.8$, Dunkley et al. 2009). The grey lines denote contours of constant α , from 10 (top right corner) to 1 (bottom left corner). The thick black

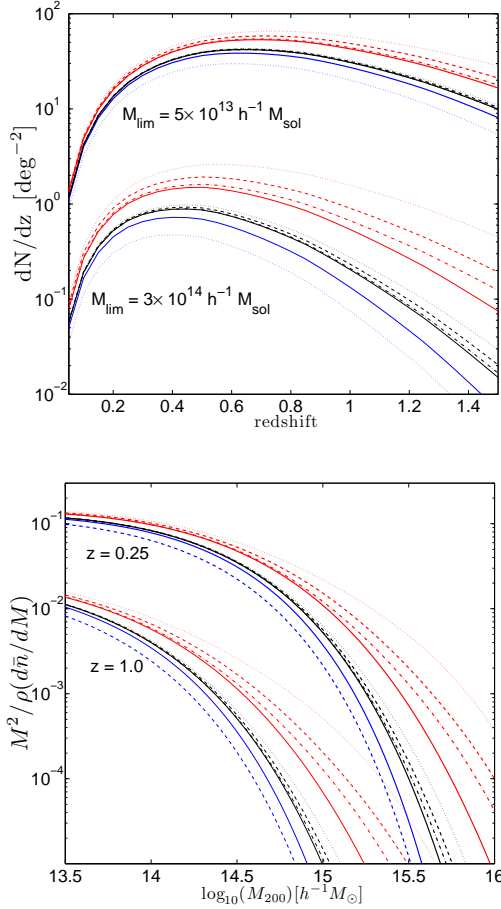


FIG. 2.— (*Upper*) The observed redshift distribution of clusters, dN/dz above a limiting observed mass threshold of $5 \times 10^{13} h^{-1} M_{\odot}$ and $3 \times 10^{14} h^{-1} M_{\odot}$. (*Lower*) The observed mass distribution of clusters $M_{\text{obs}}^2 / \rho_m (d\bar{n}/dM_{\text{obs}})$ at $z = 0.25$ and $z = 1$. In each plot, the line colors represent the value of $\sigma_{\ln M}$; 0 (blue), 0.25 (black) and 0.5 (red). The solid lines represent $\gamma = \kappa = 0$, the dashed $\gamma = 0.5, \kappa = 0$, dot-dashed $\kappa = 0.5$ ($\gamma = 0$) and the dotted line $\gamma = 1, \kappa = 1$ (in our fiducial cosmology). The blue dotted line shows the results for a WMAP3 cosmology, where $\sigma_8 = 0.77$, $\Omega_M = 0.24$, $H_0 = 73 \text{ km/s/Mpc}$, and we take $\sigma_{\ln M} = 0$.

solid and dashed contours denote $\alpha = 2$ and 4, the critical slopes α_c for DES and SPT, respectively. These contours thus give $M_c(z)$ for each survey. The vertical solid and dashed lines represent the limiting mass for each survey.

The Figure demonstrates that for the SZ survey, $\alpha \sigma_{\ln M}$ becomes greater than unity above $8 \times 10^{14} h^{-1} M_{\odot}$ at $z = 0.5$, and above $4 \times 10^{14} h^{-1} M_{\odot}$ at $z = 1$. Given the scarcity of objects above these thresholds, it is clear that γ and κ will not significantly impact the SPT cluster number counts.

For the optical survey, $M_c(z)$ is $3 \times 10^{14} h^{-1} M_{\odot}$ at $z = 0.2$, $1.7 \times 10^{14} h^{-1} M_{\odot}$ at $z = 0.5$ and $5.25 \times 10^{13} h^{-1} M_{\odot}$ at $z = 1.2$. As $M_c(z)$ remains greater than the expected limiting mass for DES, γ and κ will not strongly effect the total number of detected clusters. However, a sizeable number of clusters will be detected in mass bins that exceed $M_c(z)$. Non-Gaussian scatter in the mass-richness relation may therefore cause a detectable redistribution of clusters in mass bins greater than $M_c(z)$,

In Figure 2 we demonstrate the impact of skewness and kurtosis in $P(M_{\text{obs}}|M)$ on the observed redshift and

mass distribution of clusters. In both panels, the colors of each line represent the value of $\sigma_{\ln M}$; 0 (blue), 0.25 (black) and 0.5 (red). The solid lines represent (in our fiducial WMAP5 cosmology) $\gamma = \kappa = 0$, dashed $\gamma = 0.5, \kappa = 0$, dot-dashed $\kappa = 0.5$ ($\gamma = 0$) and dotted $\gamma = 1, \kappa = 1$ (as a more extreme scenario). The blue dotted line shows the results for a WMAP 3-year cosmology, where $\sigma_8 = 0.77$, $\Omega_M = 0.24$, $H_0 = 73 \text{ km/s/Mpc}$, and $\sigma_{\ln M} = 0$ (Spergel et al. 2007).

In the upper panel we plot the redshift distribution of clusters dN/dz using our two M_{obs} limits; $5 \times 10^{13} h^{-1} M_{\odot}$ for DES (upper lines) and $3 \times 10^{14} h^{-1} M_{\odot}$ for SPT (lower lines). For the purposes of comparison, we have plotted the results for $\sigma_{\ln M} = 0.25$ and 0.5 for both limiting masses. As predicted by Equation 10, the impact of skewness and kurtosis on the redshift distribution is dependent on the value of $\sigma_{\ln M}$ and the local slope of the (true) mass function at the limiting mass of the survey. Thus at higher redshifts the impact of γ and κ becomes greater. The flattening of dN/dz due to the higher order moments is more pronounced than that due to an increase in σ_8 or $\sigma_{\ln M}$.

For a threshold of $M_{\text{obs,lim}} = 5 \times 10^{13} h^{-1} M_{\odot}$ and $\sigma_{\ln M} = 0.5$ a skewness of γ (κ) = 0.5 increases the mean number of clusters by 10% (2%) at $z = 0.75$. The more extreme case of $\gamma = \kappa = 1$ produces a 24% increase. For the same scatter but with a limiting M_{obs} of $3 \times 10^{14} h^{-1} M_{\odot}$, γ (κ) = 0.5 increases the number of clusters at $z = 0.75$ by 42% (14%), and $\gamma = \kappa = 1$ by 218%. It is clear that it is the low mass threshold of the optical survey that prevents the higher order moments from strongly affecting the number of detected clusters in each redshift bin. The increase in dN/dz (at $z = 0.75$) for $\gamma = 0.5$ is roughly equivalent to assuming lognormal scatter but increasing $\sigma_{\ln M}$ by 22% to 0.61 (for $M_{\text{obs,lim}} = 3 \times 10^{14} h^{-1} M_{\odot}$) and by 14% to 0.57 ($M_{\text{obs,lim}} = 5 \times 10^{13} h^{-1} M_{\odot}$). For our extreme case of $\gamma = \kappa = 1$, the results are equivalent to increasing $\sigma_{\ln M}$ to 0.73 and 0.65 at each mass threshold, respectively.

For the SZ survey ($\sigma_{\ln M} = 0.25$, $M_{\text{obs,lim}} = 3 \times 10^{14} h^{-1} M_{\odot}$), increasing γ from 0 to 0.5 provides a 8% increase in the number counts at $z = 0.75$. This is equivalent to an increase in $\sigma_{\ln M}$ for purely lognormal scatter of 12% (to 0.28). The same change in kurtosis provides less than a one percent change in the number counts. The $\gamma = \kappa = 1$ case provides a 20% increase in the number counts, equivalent to an increase of $\sigma_{\ln M}$ by 28% to 0.32.

In the lower panel of Figure 2 we plot the mass distribution of detected clusters, $M_{\text{obs}}^2 / \rho_m (d\bar{n}/dM_{\text{obs}})$ (scaled to reduce the dynamic range, where ρ_m is the mean matter density of the Universe at each redshift) at $z = 0.25$ and 1.0. The line types and colors represent the same values of $\sigma_{\ln M}$, γ , and κ as the upper plot. For integrated SZ flux (for which $\sigma_{\ln M} = 0.25$), the higher-order moments do not have a significant effect on the shape of the mass function. The impact of γ and κ is more evident for high-scatter mass indicators (red lines), flattening the mass distribution above $10^{14.5} h^{-1} M_{\odot}$ at $z = 0.25$, and $10^{14} h^{-1} M_{\odot}$ at $z = 1.0$. These masses roughly correspond to the predicted values of $M_c(z)$ at these redshifts in Figure 1 ($\alpha = 2$ contour).

Overall, Figure 2 demonstrates two points. A skewness

of $\gamma = 0.5$ has the same effect on dN/dz (at $z = 0.75$) as increasing the variance $\sigma_{\ln M}^2$ by 0.075 for DES and by 0.016 for SPT. For the significantly more non-Gaussian distribution parameterised by $\gamma = \kappa = 1$, the equivalent change in $\sigma_{\ln M}^2$ is 0.17 for DES and 0.04 for SPT. Lima & Hu (2005) show that a prior of $\sigma(\sigma_{\ln M}^2) = 0.01$ is necessary to ensure that uncertainty on the level of scatter does not degrade the constraints that can be placed on the dark energy equation of state parameter w (see their Figure 6). Therefore, assuming γ does not greatly exceed 0.5, non-Gaussian scatter in the mass-SZ flux scaling relation should not significantly degrade the cosmological constraints that can be achieved by SPT. However, for surveys utilizing a high-scatter mass proxy such as optical richness, an unknown level of non-Gaussianity in $P(M_{\text{obs}}|M)$ may limit the constraints that can be placed on the dark energy equation of state via cluster number counts.

Secondly, if one aims to use the shape of the mass function to self-calibrate a survey to obtain information on the slope, normalization and variance of the mass-observable scaling relation, then care must be taken to ensure that the parameters are not biased due to the increasing impact of the higher order moments on the shape of the mass function towards high masses. One means of ensuring this is to include only a single mass bin for $M_{\text{obs}} > M_c(z)$.

4. CONCLUSION

We have investigated the impact of non-Gaussian scatter in the mass-observable scaling relation on the cluster mass function by incorporating the third and fourth moments (skewness and kurtosis) into the probability distribution $P(M_{\text{obs}}|M)$ via the Edgeworth expansion. We have demonstrated that if $\alpha\sigma_{\ln M}$ – the product of the standard deviation in $P(M_{\text{obs}}|M)$ and the slope of the mass function at the limiting mass of a survey – is greater than unity, then positive skewness and kurtosis will increase the number of clusters detected and flatten the high-mass end of the observed mass function.

For low scatter mass proxies like integrated SZ flux, higher order moments do not significantly affect the mass

and redshift distribution of clusters. However, for surveys utilizing a high scatter mass proxy such as optical richness, the limiting mass threshold must be less than $10^{14}h^{-1}M_{\odot}$ to ensure that the skewness does not significantly effect dN/dz , especially at high redshift. We have also found that an unknown level of non-Gaussian scatter is roughly equivalent to an additional uncertainty on the variance $\sigma_{\ln M}^2$ in $P(M_{\text{obs}}|M)$ and thus may limit the constraints that can be placed on the dark energy equation of state parameter w , especially for surveys that use a high scatter mass proxy. Furthermore, if one wishes to use the shape of the mass function in each redshift bin to self-calibrate for cluster scaling relation parameters then it will be necessary to account for non-Gaussian scatter on the shape of the mass function by marginalising over the skewness and kurtosis parameters, γ and κ in addition to the the variance $\sigma_{\ln M}^2$, slope and normalisation in each redshift bin.

We note that the values of γ and κ used in the examples given in this work were chosen arbitrarily (and to be small enough to ensure that the Edgeworth expansion remains an appropriate approximation to a non-Gaussian $P(M_{\text{obs}}|M)$). Large-volume simulations and mock-galaxy catalogues containing several thousands of clusters will be necessary to obtain better motivated predictions of γ and κ for optical, SZ (and X-ray) surveys. Measuring γ and κ would require a large observational sample with precisely measured masses (for example, using X-ray spectroscopic temperatures). However, the higher order statistics are strongly influenced by rare, outlying objects (e.g. major mergers), or the impact of observational selection effects such as cluster-cluster confusion. For this reason, it is unlikely that it will be possible to place tight priors on these parameters.

5. ACKNOWLEDGMENTS

This work is supported by NSERC through the Discovery Grant Awards to GPH. GPH would also like to acknowledge support from the Canadian Institute for Advanced Research and the Canada Research Chairs Program. We would like to thank Jochen Weller, Gus Evrard and Eduardo Rozo for useful discussions.

REFERENCES

- Bahcall, N. & Fan, X. 1998, *ApJ*, 504, 1
 Becker, M. R., McKay, T. A., Koester, B., Wechsler, R. H., Rozo, E., Evrard, A., Johnston, D., Sheldon, E., Annis, J., Lau, E., Nichol, R., & Miller, C. 2007, *ApJ*, 669, 905
 Bernardeau, F. & Kofman, L. 1995, *ApJ*, 443, 479
 Blinnikov, S. & Moessner, R. 1998, *A&AS*, 130, 193
 Cohn, J. D., Evrard, A. E., White, M., Croton, D., & Ellingson, E. 2007, *MNRAS*, 382, 1738
 Cunha, C. 2009, *Phys. Rev. D*, 79, 063009
 Dunkley, J., Komatsu, E., Nolta, M. R., Spergel, D. N., Larson, D., Hinshaw, G., Page, L., Bennett, C. L., Gold, B., Jarosik, N., Weiland, J. L., Halpern, M., Hill, R. S., Kogut, A., Limon, M., Meyer, S. S., Tucker, G. S., Wollack, E., & Wright, E. L. 2009, *ApJS*, 180, 306
 Eke, V. R., Cole, S., Frenk, C. S., & Patrick Henry, J. 1998, *MNRAS*, 298, 1145
 Evrard, A. E., Bialek, J., Busha, M., White, M., Habib, S., Heitmann, K., Warren, M., Rasia, E., Tormen, G., Moscardini, L., Power, C., Jenkins, A. R., Gao, L., Frenk, C. S., Springel, V., White, S. D. M., & Diemand, J. 2008, *ApJ*, 672, 122
 Haiman, Z., Mohr, J. J., & Holder, G. P. 2001, *ApJ*, 553, 545
 Hallman, E. J., O’Shea, B. W., Burns, J. O., Norman, M. L., Harkness, R., & Wagner, R. 2007, *ApJ*, 671, 27
 Holder, G. P., McCarthy, I. G., & Babul, A. 2007, *MNRAS*, 382, 1697
 Hu, W. 2003, *Phys. Rev. D*, 67, 081304
 Jenkins, A., Frenk, C. S., White, S. D. M., Colberg, J. M., Cole, S., Evrard, A. E., Couchman, H. M. P., & Yoshida, N. 2001, *MNRAS*, 321, 372
 Lima, M. & Hu, W. 2004, *Phys. Rev. D*, 70, 043504
 —. 2005, *Phys. Rev. D*, 72, 043006
 Majumdar, S. & Mohr, J. J. 2003, *ApJ*, 585, 603
 Perlmutter, S., Aldering, G., Goldhaber, G., Knop, R., Nugent, P., Castro, P., Deustua, S., Fabbro, S., Goobar, A., Groom, D. E., Hook, I. M., Kim, A. G., Kim, M., Lee, J., Nunes, N., Pain, R., Pennypacker, C., Quimby, R., Lidman, C., Ellis, R., Irwin, M., McMahon, R., Ruiz-Lapuente, P., Walton, N., Schaefer, B., Boyle, B., Filippenko, A., Matheson, T., Fruchter, A., Panagia, N., Newberg, H. J. M., & Couch, W. 1999, *ApJ*, 517, 565
 Pratt, G. W., Croston, J. H., Arnaud, M., & Böhringer, H. 2009, *A&A*, 498, 361
 Rozo, E., Rykoff, E. S., Evrard, A., Becker, M., McKay, T., Wechsler, R. H., Koester, B. P., Hao, J., Hansen, S., Sheldon, E., Johnston, D., Annis, J., & Frieman, J. 2009, *ApJ*, 699, 768

- Rozo, E., Rykoff, E. S., Koester, B. P., McKay, T., Hao, J., Evrard, A., Wechsler, R. H., Hansen, S., Sheldon, E., Johnston, D., Becker, M., Annis, J., Bleem, L., & Scranton, R. 2008, ArXiv e-prints
- Rykoff, E. S., Evrard, A. E., McKay, T. A., Becker, M. R., Johnston, D. E., Koester, B. P., Nord, B., Rozo, E., Sheldon, E. S., Stanek, R., & Wechsler, R. H. 2008a, MNRAS, 387, L28
- Rykoff, E. S., McKay, T. A., Becker, M. R., Evrard, A., Johnston, D. E., Koester, B. P., Rozo, E., Sheldon, E. S., & Wechsler, R. H. 2008b, ApJ, 675, 1106
- Schmidt, B. P., Suntzeff, N. B., Phillips, M. M., Schommer, R. A., Clocchiatti, A., Kirshner, R. P., Garnavich, P., Challis, P., Leibundgut, B., Spyromilio, J., Riess, A. G., Filippenko, A. V., Hamuy, M., Smith, R. C., Hogan, C., Stubbs, C., Diercks, A., Reiss, D., Gilliland, R., Tonry, J., Maza, J. e., Dressler, A., Walsh, J., & Ciardullo, R. 1998, ApJ, 507, 46
- Shaw, L. D., Holder, G. P., & Bode, P. 2008, ApJ, 686, 206
- Shaw, L. D., Weller, J., Ostriker, J. P., & Bode, P. 2006, ApJ, 646, 815
- Spergel, D. N., Bean, R., Doré, O., Nolta, M. R., Bennett, C. L., Dunkley, J., Hinshaw, G., Jarosik, N., Komatsu, E., Page, L., Peiris, H. V., Verde, L., Halpern, M., Hill, R. S., Kogut, A., Limon, M., Meyer, S. S., Odegard, N., Tucker, G. S., Weiland, J. L., Wollack, E., & Wright, E. L. 2007, ApJS, 170, 377
- Stanek, R., Rasia, E., Evrard, A. E., Pearce, F., & Gazzola, L. 2009, in preparation
- Tinker, J., Kravtsov, A. V., Klypin, A., Abazajian, K., Warren, M., Yepes, G., Gottlöber, S., & Holz, D. E. 2008, ApJ, 688, 709
- Warren, M. S., Abazajian, K., Holz, D. E., & Teodoro, L. 2006, ApJ, 646, 881
- Weller, J., Battye, R., & Kneissl, R. 2001, Phys. Rev. Lett., 88, 231301
- White, M., Hernquist, L., & Springel, V. 2002, ApJ, 579, 16